Design Tradeoffs in Multi-Pole NEM Relays for Reconfigurable Datapath Routing

ENGR 241 Final Project

Akash Levy, Dylan Woodhead

December 9, 2019

Abstract

In this work, we design and optimize the physical and electrical properties of multi-pole single-throw NEM relays for use as reconfigurable routers. Prior work has examined the use of single-pole NEM relays as routers for field-programmable gate arrays (FPGAs). However, no realistic scheme for integrating the routers in 3D was presented, so the prior results represent optimistic estimates. We describe a realistic process flow for fabricating reconfigurable NEM routers on top of back-end-of-line CMOS layers. We then develop a parametric OpenSCAD model describing the layout of a NEM relay, and analyze our design's physical and electrical properties using FreeCAD finite element modelling (FEM) and approximate analytical calculations. We explore the design tradeoffs based on our findings from FEM and analytical models.

1 Introduction

Field-programmable gate arrays (FPGAs) are programmable logic devices (PLDs) that enable rapid prototyping of digital circuits and provide an alternative to the expensive application-specific integrated circuit (ASIC) design process today. However, when compared with ASICs performing the same function, SRAM-based FPGAs typically have 10-40 times lower logic density, 3-4 times higher delay, and 5-12 times higher dynamic power dissipation [8] [12] [13]. This is because reconfigurable components incur large overhead—instead of being packed tightly, configurable logic blocks (CLBs) in FPGAs are laid out relatively far apart to make space for routing components, resulting in greater interconnect delay, power dissipation, and chip area. The disparity in the performance of FPGAs and ASICs provides motivation to find ways to reduce reconfigurability overhead, so that ultimately PLDs can become competitive with ASICs at manufacturing scale. Possible solutions lie with PLD designs that trade off fine-grained CLBs with more specialized blocks e.g. coarse-grained reconfigurable arrays (CGRAs) [11], or with emerging nanotechnologies that enable novel design strategies in the space of reconfigurable computing devices.

In this work, we model the properties of multi-pole single-throw nanoelectromechanical (NEM) relays as reconfigurable routers for PLDs. Prior work at Stanford has examined the use of single-pole NEM relays as programmable routers in FPGAs [3]. However, no realistic scheme for integrating the relays in 3D was provided in that work, so the prior estimates are certainly optimistic. Here, we focus on analyzing and optimizing a specific relay technology for use in programmable routing: 4-terminal, out-of-plane, n-type poly-SiGe relays largely inspired by those developed at Berkeley (shown in Figure 1) [10]. Relays of this type are chosen due to their desirable properties as routers: (1) they can be monolithically integrated in 3-D on top of CMOS BEOL layers, (2) they effectively decouple actuation (body and gate) and signal (source and drain), (3) they can operate at reasonable voltages ($< 10\,\mathrm{V}$), and (4) they have been shown

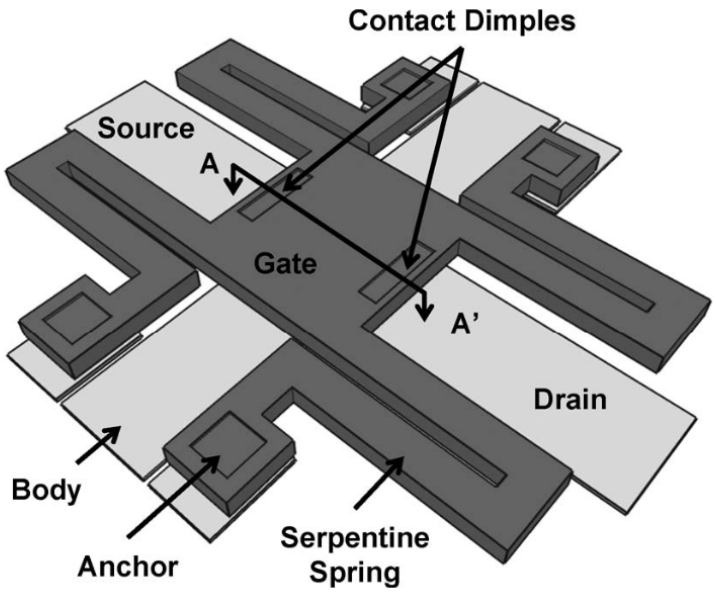

Figure 1: Schematic 3-D view of the Berkeley design for an electrostatically-actuated 4T relay structure. Adapted from [7].

to exhibit low contact resistance ($< 1\,\mathrm{k}\Omega$) with reasonable endurance ($> 10^6$) [9]. We modify the Berkeley relay design in two ways; first, we modify the layout, as shown in Figure 2, to obtain circular displacement contours. This change allows for easy placement of multiple contacts in an optimal fashion. Second, we increase the size of the contacts—instead of using tiny dimples, we have larger rectangular contacts that enable reduced contact resistance. Otherwise, the process flow for relay fabrication is essentially the same as that described in [10]. While the Berkeley relay designs have focused on up to four poles, we examine the limits of bit width scalability

2 Background and Previous Work

With technology scaling, it is becoming increasingly difficult to design FPGAs using NMOS pass transistors for programmable routing. An NMOS pass transistor introduces a threshold (V_t) drop when passing high voltage level, after which the voltage level must be restored. Unfortunately, pass transistor threshold voltage (V_t) cannot be further reduced due to leakage power constraints.

NEM relays are switches that are actuated electrostatically at the nanoscale. Their properties have been studied in depth, and they have gained interest for their potential as pass transistor replacements in FPGAs [2] [3]. NEM relays have extremely low static power dissipation and low ON-state resistance—however, they switch much slower than transistors (on the order of nanoseconds) and typically operate at higher voltages. NEM relays have a sharp I_{DS}-V_G curve and also exhibit hysteresis in switching state based on applied gate voltage (V_G). This has led to NEM relay-based SRAM designs utilizing this property (though these will not be discussed in depth here).

There are two kinds of NEM relays that are of interest for reconfigurable routing: 3-terminal (3T) and 4-terminal (4T) devices (see Figure 2). 3T devices have a source, drain, and gate, and the voltage that controls the beam is the voltage between the gate and source. This means that the source voltage affects the beam state, which is undesirable for a device that needs to behave as a pass transistor. The 4T device mitigates this problem by having the beam

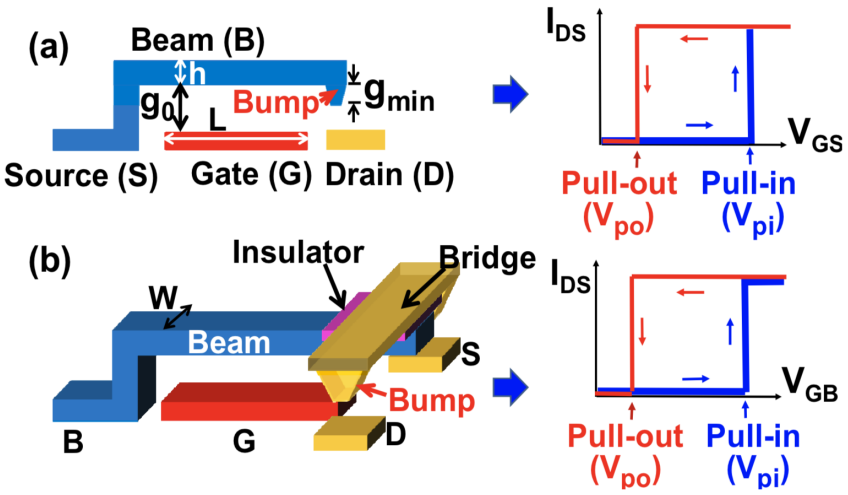

Figure 2: Figure adapted from [3]. (a) A 3T NEM relay and its I_{DS}-V_{GS} characteristics; (b) A 4T NEM relay and its I_{DS}-V_{GB} characteristics. The beam is insulated from the bridge for S/D contacts [4].

electrically isolated from the "bridge" that connects the source and drain [10]. NEM relays can be fabricated at low-temperatures ($< 400\,°C$) making them compatible with CMOS back-end-of-line (BEOL) processes, and they make use of materials already available in foundries. Simple lateral designs require 4-7 masks at the top layer of the device [5]. Research into scaling these devices to smaller sizes and integrating them in 3-dimensions is an ongoing effort.

3 Process Flow for Monolithic 3D Integration of NEM Relays

The process flow for fabricating the relays is given in Figure 3. All of the processing steps are CMOS-compatible—they occur at $< 400\,°C$ and use materials that are not destructive to CMOS components (i.e. no Au is used, as this is a minority-carrier killer that can destroy the functionality of MOSFET channels). The process uses 5 masks: the first is for defining the contact pads, the second is for defining the W dimples, the third is for defining the connections from the W dimples to the anchors, the fourth is for defining the relay shape, and the fifth is for defining the anchors (not shown in the process flow of Figure 3).

4 Parametric NEM Relay Design

We developed our 4T NEM relay design in OpenSCAD with adjustable parameters to allow us to configure the relay design and analyze the effects of tweaking different dimensions of the system. An example layout is given in Figure 4. 14 different parameters are available in our parametric design. Of these 14, we constrained four parameters to reduce the design space. The relay cantilever length was set to be equal to the side length of the plate for all variants tested. The gap between the cantilever and the plate was also constrained to be equal to the width of the cantilever. Although this parameter affects the spring constant of the relay, we chose not to analyze the effects of changing it. The thickness of the substrate and of the Al_2O_3 layer was set to be the same in all the models as well.

We built the model with an actuation gap parameter that allows us to modify the distance between the source and the drain. This parameter mainly affects height of the anchors. We also control the thickness and the length of the poly-SiGe layer. These parameters control both the proof mass of the relay and the effective area of electrostatic actuation. Although we chose not

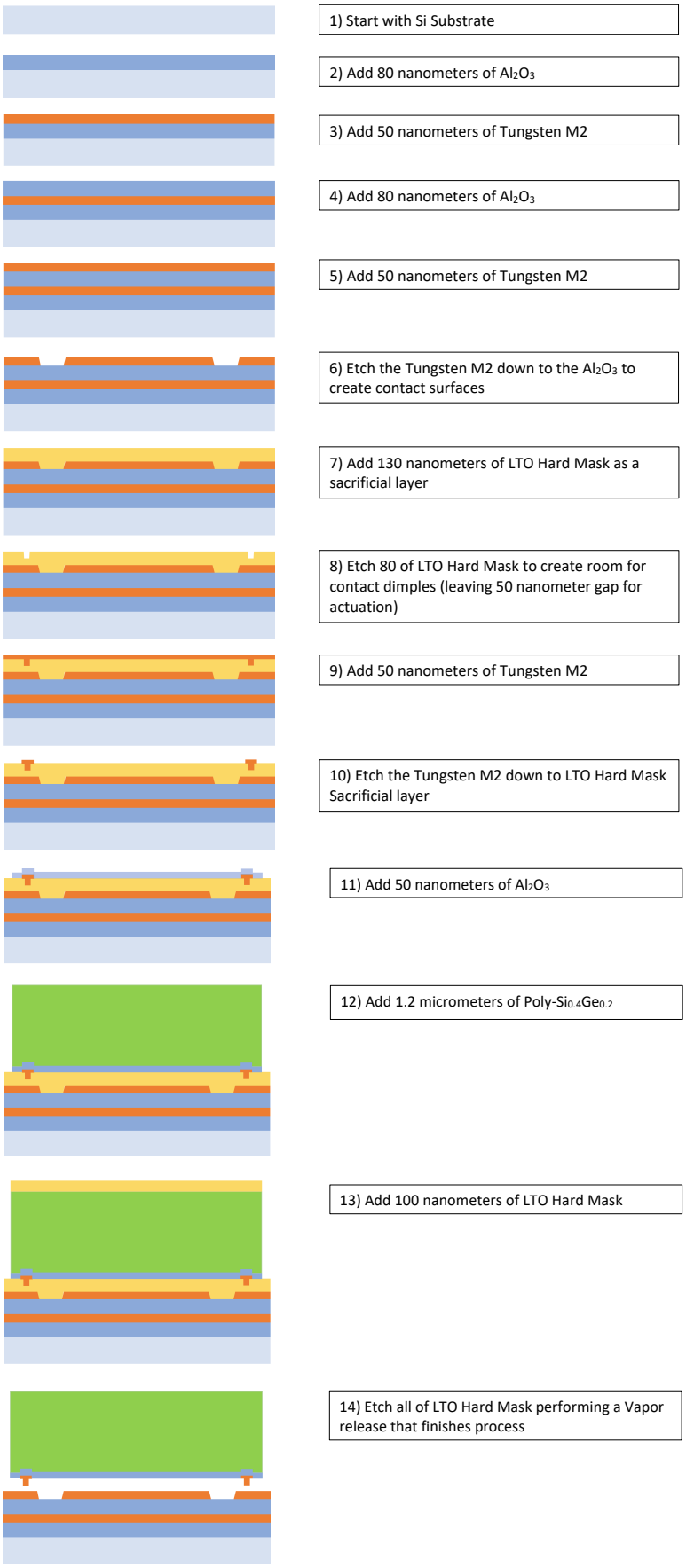

Figure 3: Illustration of the process flow for fabricating multi-pole NEM relays for programmable routing.

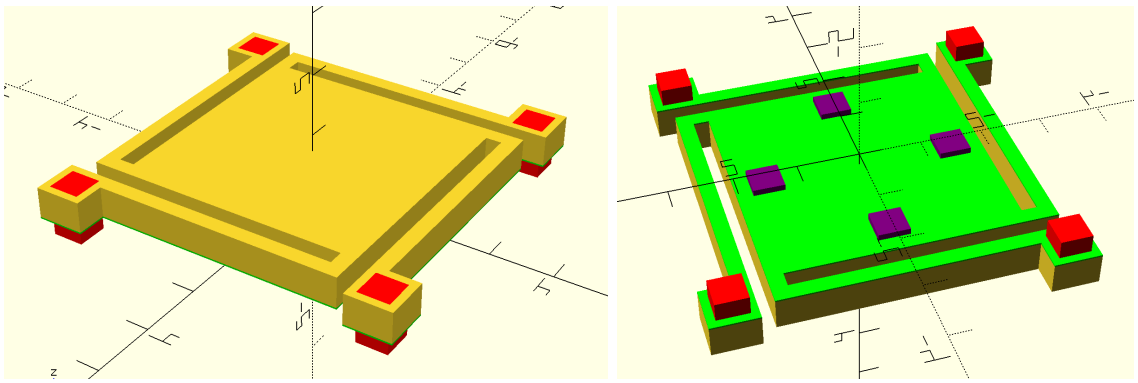

Figure 4: An example layout of our 4T parametric NEM relay design in OpenSCAD.

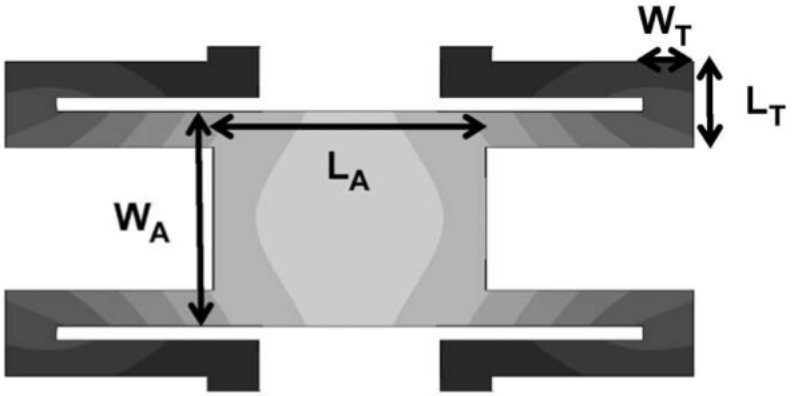

Figure 5: Adapted from [7]. Berkeley relay layout and resulting non-circular displacement contours.

to change the length of the cantilever independently of the relay width, we analyze the effects of a changing cantilever thickness. This parameter has a significant impact on the spring constant of the cantilever.

The number of contact dimples and their location on the underside of the relay have an impact on the system's properties. We place the dimples with circular symmetry along the bottom, meaning all dimples are equidistant from the center of the relay. The circular symmetry forces all of the contacts to be on the same plane during z-direction displacement, creating a balanced relay with equal force at each contact. By contrast, the original Berkeley NEM relay design has non-circular displacement contours as shown in Figure 5. The OpenSCAD model can also control the length and thickness of each contact. The side length parameter affects both the contact resistance and the contact-substrate capacitance which is a signal-dependent force. The thickness parameter impacts the size of the actuation gap.

By varying parameters in different models and performing Finite Element Analysis on their structure, we were able to better understand the effects each parameter has on the NEM relay.

4.1 Default Relay Parameters

Below is the OpenSCAD code for the default relay parameters:

```
// RELAY PARAMETERS (lengths are in units of um)
g_act = 0.08;                // actuation gap: gap between

t_poly = 0.2;                // thickness of poly-SiGe layer
```

```
L_plate = 5;                // side length of parallel plate

L_cant = L_plate;           // length of cantilever
W_cant = 0.2;               // width of cantilever
g_cant = W_cant;            // gap between plate and cantilever

L_via = 0.5;                // side length of via
L_anc = L_via + 0.25;       // side length of anchor attachment

n_cont = 4;                 // number of contacts
L_cont = 0.5;               // side length of contact
r_cont = 1.5;               // radius of circle along which to place contacts
t_cont = 0.04;              // thickness of contact

t_sub = 0.1;                // substrate thickness

t_sp = 0.025;               // thickness of spacer
```

5 Modelling of NEM Relay Characteristics

5.1 Approximate Analytical Models of NEM Relay Design

To facilitate approximate analytical modelling, we start by finding the mechanical properties of the materials we are using. From [7], we obtain the Young's modulus, the shear modulus, and density of the poly-Si structural layer that determines most of the mechanical properties of the relay:

$$E_{poly} = 145\,\text{GPa} \qquad G_{poly} = 57\,\text{GPa} \qquad \rho_{poly} = 4126\,\text{kg/m}^3 \tag{1}$$

In our parametric relay design, we have (for now) constrained our design by making the cantilever length equal to the plate length:

$$L_{cant} = L_{plate} \tag{2}$$

We know the areas of both our plate and our contacts:

$$A_{plate} = L_{plate}^2 \qquad A_{cont} = L_{cont}^2 \tag{3}$$

We also assume some shielding of the electrostatic force between the relay and the body by the contacts. Thus, we use an *effective* area of electrostatic actuation, which is given by subtracting the total contact area from the total plate area:

$$A_{act} = A_{plate} - N_{cont}A_{cont} \tag{4}$$

Using these, we can compute the approximate force between the substrate and the relay with a parallel plate capacitor model. We first model the simplest case in which all our contacts are grounded, in which case they do not generate any force. Hence our total upward force is minimized and determined solely by the parallel plates of the relay and the body contact:

$$\boxed{F_{E,min} \approx \frac{\epsilon_0 A_{act} V_{gb}^2}{2(g_{act} - x)^2}} \tag{5}$$

The other extreme case occurs when all of the contacts are carrying a high logical value i.e. V_{dd}. In this case, there is an additional force on the relay from the contacts, and the combined upward force from the contacts and the relay is maximized. We will not focus in detail on this

case, and will instead assume that V_{dd} is small enough that $F_{E,min} = F_{E,max}$. The equation for $F_{E,max}$ complicates the analysis with the addition of an extra term:

$$\boxed{F_{E,max} \approx \frac{\epsilon_0 A_{act} V_{gb}^2}{2(g_{act} - x)^2} + \frac{\epsilon_0 N_{cont} A_{cont} V_{dd}^2}{2(g_{act} - t_{cont} - x)^2}} \tag{6}$$

Now we have to solve for the spring constants that define the restoring force for the relay. We model the springs as 4 two-part cantilevers in parallel. Each two-part cantilever consists of two beams in series, having lengths:

$$L_{c1} = (L_{cant} - W_{cant}/2)/2 \qquad L_{c2} = 3W_{cant}/4 \tag{7}$$

Then, using the clamped-guided beam approximation for each of these beams, we can compute the approximate spring constants for each piece based on the dimensions and material parameters:

$$k_{c1} = \frac{E_{poly} W_{cant} t_{poly}^3}{4L_{c1}^3}/2 \qquad k_{c2} = \frac{E_{poly} W_{cant} t_{poly}^3}{4L_{c2}^3}/2 \tag{8}$$

The total spring constant is found using the parallel/series spring formulas:

$$k_{tot} \approx 4 \times \frac{1}{1/k_{c1} + 1/k_{c2}} \tag{9}$$

When simplified, this becomes:

$$\boxed{k_{tot} \approx \frac{E_{poly} W_{cant} t_{poly}^3}{2(L_{c1}^3 + L_{c2}^3)}} \tag{10}$$

We then compute the proof mass of the relay, ignoring the mass from the cantilevers, contacts, and insulating spacer layer:

$$\boxed{M \approx \rho_{poly} A_{plate} t_{poly}} \tag{11}$$

Now we have all the components to determine the equation of motion for the relay's displacement using Newton's laws:

$$\boxed{M\ddot{x} = F_{net} = F_E(x) - k_{tot} x} \tag{12}$$

We can perform stability analysis to determine at what $x = x_{pi}$ the beam pulls in. If we decrement the gap x by Δx, the increment ΔF_{net} must be greater than 0 or the pull-in phenomenon occurs:

$$\Delta F_{net} = \frac{\partial F_{net}}{\partial x}\, \Delta x = \frac{\partial}{\partial x} \left(F_E(x) - k_{tot} x\right) \Delta x > 0 \tag{13}$$

We assume all contacts are grounded i.e. $F_E(x) = F_{e,min}(x)$:

$$\Delta F_{net} = \left(\frac{\epsilon_0 A_{act} V_{gb}^2}{(g_{act} - x_{pi})^3} - k_{tot} \right) \Delta x \tag{14}$$

For pull-in to occur, we thus have:

$$k_{tot} = \frac{\epsilon_0 A_{act} V_{gb}^2}{(g_{act} - x_{pi})^3} \tag{15}$$

Now we can plug this value of k_{tot} into the equation for $F_{net} = 0$. This determines at what point, x_{pi}, the forces are balanced and the pull-in phenomenon is observed:

$$F_{tot} = F_E(x_{pi}) - k_{tot} x_{pi} = \frac{\epsilon_0 A_{act} V_{gb}^2}{2(g_{act} - x_{pi})^2} - \frac{\epsilon_0 A_{act} V_{gb}^2}{(g_{act} - x_{pi})^3} x_{pi} = 0 \tag{16}$$

$$\frac{x_{pi}}{g_{act} - x_{pi}} = \frac{1}{2} \tag{17}$$

$$\boxed{x_{pi} = \frac{g_{act}}{3}} \tag{18}$$

We then determine the pull-in voltage by plugging x_{pi} into our equations for k_{tot} and solving for $V_{gb} = V_{pi}$:

$$k_{tot} = \frac{\epsilon_0 A_{act} V_{pi}^2}{(g_{act} - x_{pi})^3} = \frac{\epsilon_0 A_{act} V_{pi}^2}{(2g_{act}/3)^3} \tag{19}$$

$$\boxed{V_{pi} = \sqrt{\frac{8 k_{tot} g_{act}^3}{27 \epsilon_0 A_{act}}}} \tag{20}$$

To determine the pull-out voltage, V_{po}, we assume some amount of adhesion of the contacts. For TiO_2-coated W contacts, in [7], the adhesion force is extracted to be 0.45 µN for a contact area of 20 µm^2. For now, we approximate that the adhesion force is proportional to contact area:

$$F_A = \frac{0.45\,\mu\text{N}}{20\,\mu\text{m}^2} N_{cont} A_{cont} = (22\,500\,\text{N/m}^2) N_{cont} A_{cont} \tag{21}$$

Now we have a new equation of motion describing the case where the relay starts in the ON position, i.e. $x = t_{cont}$:

$$M\ddot{x} = F_{net} = F_E(t_{cont}) + F_A - k_{tot} t_{cont} \tag{22}$$

Solving for $V_{gb} = V_{po}$ when $F_{net} = 0$, yields:

$$F_{net} = \frac{\epsilon_0 A_{act} V_{po}^2}{2(g_{act} - t_{cont})^2} + F_A - k_{tot} t_{cont} = 0 \tag{23}$$

$$\boxed{V_{po} = \sqrt{\frac{2(k_{tot} t_{cont} - F_A)(g_{act} - t_{cont})^2}{\epsilon_0 A_{act}}}} \tag{24}$$

Finally, we model our approximate expected contact resistance based on the *effective contact area* model [6] [1].

$$\boxed{R_{cont} = \frac{4 \rho_W \lambda_W}{3 A_r}} \tag{25}$$

In the equation above, ρ_W is the resistivity of the W contact, A_r is the effective area of the contact, and λ_W is the electron mean free path in the W contact. The effective area of the contact (which is typically dominated by asperities) is a function of the loading force, which is F_{net} from earlier, the material hardness (H), and the deformation coefficient (ξ) at the contact. We assume the relay is operating at an overdrive voltage of $V_{gb} = 1.1 V_{pi}$ to determine the effective contact area:

$$A_r \approx \frac{F_{net}(x = t_{cont}, V_{gb} = 1.1 V_{pi})}{\xi_W H_W} \tag{26}$$

We use the following parameters in our analysis:

$$H_W = 1.1\,\text{GPa} \qquad \lambda_W = 33\,\text{nm} \qquad \rho_W = 55\,\text{n}\Omega\,\text{m} \qquad \xi_W \approx 0.3 \text{ (elastic contact)} \tag{27}$$

For our default relay design with parameters as described in the previous section, we obtain:

Proof mass: 2.063×10^{-14} kg
Spring constant: 7.886 N/m
Pull-in voltage: 2.373 V

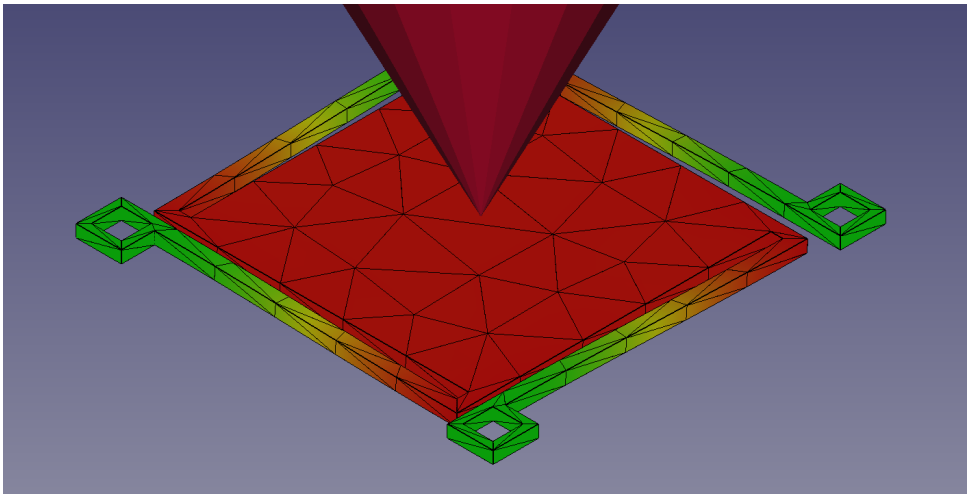

Figure 6: Finite element analysis capturing the effect of a 10 nN force on the parametric NEM relay. The maximum z-displacement (color-coded) is used to compute the spring constant.

Pull-out voltage: 2.100 V
Contact resistance: 23.33 Ω

The pull-in and pull-out voltages are within the range of CMOS I/O circuitry which is ideal for closely integrating these relays with CMOS components. The predicted contact resistance is low enough that there is unlikely to be a huge issue with the signal propagation through the relays.

5.2 Finite Element Analysis of NEM Relay Design

We perform finite element analysis to confirm the correctness of our analytical models in predicting spring constants. We export the poly-SiGe layers of our OpenSCAD designs for modelling. We place a small force constraint on the top face of our relay and find the maximum displacement, then divide the force by the displacement to compute an approximate spring constant. The force used for most of our designs is 10 nN (we adjust the force manually for the cases where the spring constant is too high or low for the FEM tool to show meaningful results). We then perform meshing of our STL designs after conversion to FreeCAD solids. The meshing is done with Netgen using an optimized very-coarse mesh. Analysis of the system dynamics is performed with CalculiX—an example of the mesh under force is given in Figure 6.

5.3 Modelling Results and Comparison

We model the effects of varying several parameters in our design: actuation gap, contact side length, relay side length, contact thickness, poly-SiGe thickness, and cantilever width. In particular, we model the effects of these parameters on the pull-in/pull-out voltages, contact resistance, and spring constants. For spring constants, we also provide a comparison between FEM and our analytical models where relevant.

5.3.1 Actuation Gap

The actuation gap does not affect the spring constant of the relay. However, it affects the contact resistance and pull-in and pull-out voltage as shown in Figure 7. The contact resistance is maximized when the electrostatic actuation force and spring forces are balanced. At

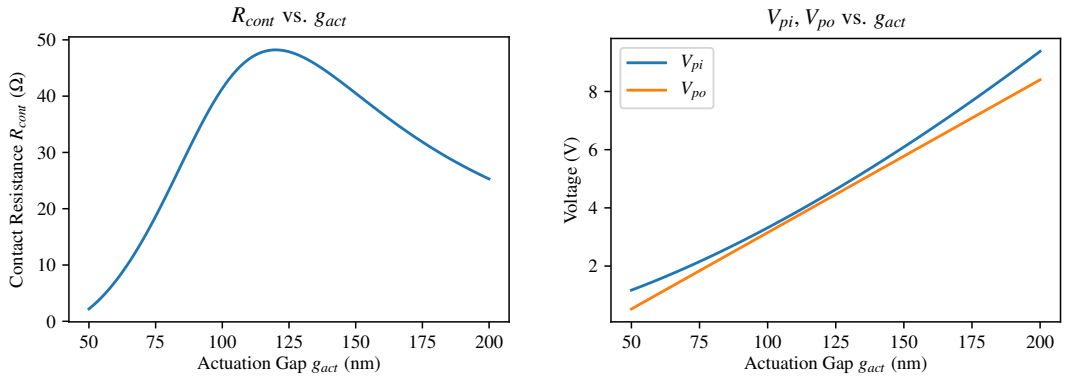

Figure 7: (Left) Contact resistance of relay vs. actuation gap. (Right) Pull-in/pull-out voltage vs. actuation gap. All other parameters are set to defaults.

this point, the force pressing down from the plate is minimized and the contact resistance is hence maximized. The pull-in and pull-out voltages monotonically increase as a function of the actuation gap. This makes sense since the larger the actuation gap, the larger the electrostatic force needed to overcome the spring's restoring force. Interestingly, the hysteresis is minimized at the same point the contact resistance is maximized—this is the same point at which the electrostatic force and spring forces are balanced. This shows that there is a definite trade-off between contact resistance and hysteresis window (at least as contact resistance is predicted by the effective contact area model).

5.3.2 Contact Side Length

The contact side length controls the total contact area. This has no effect on the spring constant, but has an impact on the effective actuation area and contact stiction. As a result of modifying the effective actuation area, the pull-in/pull-out voltages change as shown in Figure 8. We see that the pull-in voltage increases and the pull-out voltage decreases. The pull-in voltage increase can be explained by the reduced actuation area that reduces the force between the relay and the body. The pull-out voltage decrease can be explained by the increase in contact stiction—a larger contact area increases stiction and so the voltage needs to drop further than before for the relay to pull out.

5.3.3 Relay Side Length

The cantilever beam length is constrained to be equal to the relay side length. It directly controls the effective electrostatic actuation area. Indirectly (through its impact on the cantilever beam length), it controls the spring constant of the relay. Figure 9 shows plots of the effects. We see that the spring constant is reduced with relay side length—this makes sense because the cantilever beam is getting longer. We also observe a good match between the analytical predictions and the FEM results, especially at larger areas. The contact resistance increases as a result of plate length. This is because of the decrease in the spring constant, which leads to a decrease in the pull-in and pull-out voltages, which in turn leads to lower electrostatic force since we operate at $V_{gb} = 1.1V_{pi}$. This lower electrostatic force results in a larger contact resistance.

5.3.4 Contact Thickness

The contact thickness does not affect the spring constant of the relay. However, it affects the contact resistance and pull-in and pull-out voltages as shown in Figure 10. The mechanism for

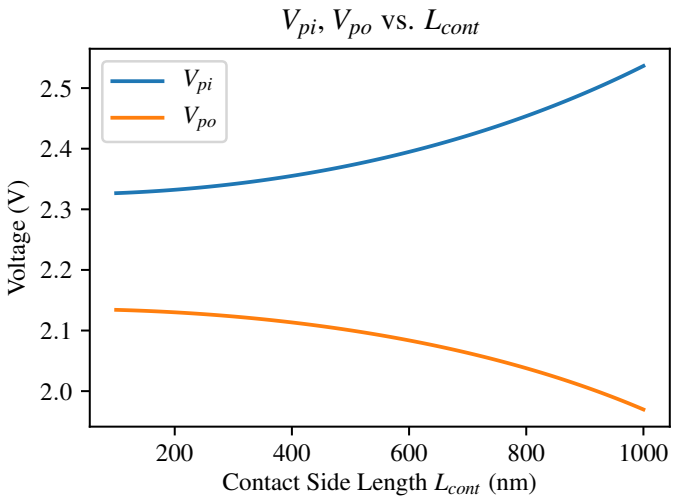

Figure 8: Pull-in/pull-out voltage vs. contact side length. All other parameters are set to defaults.

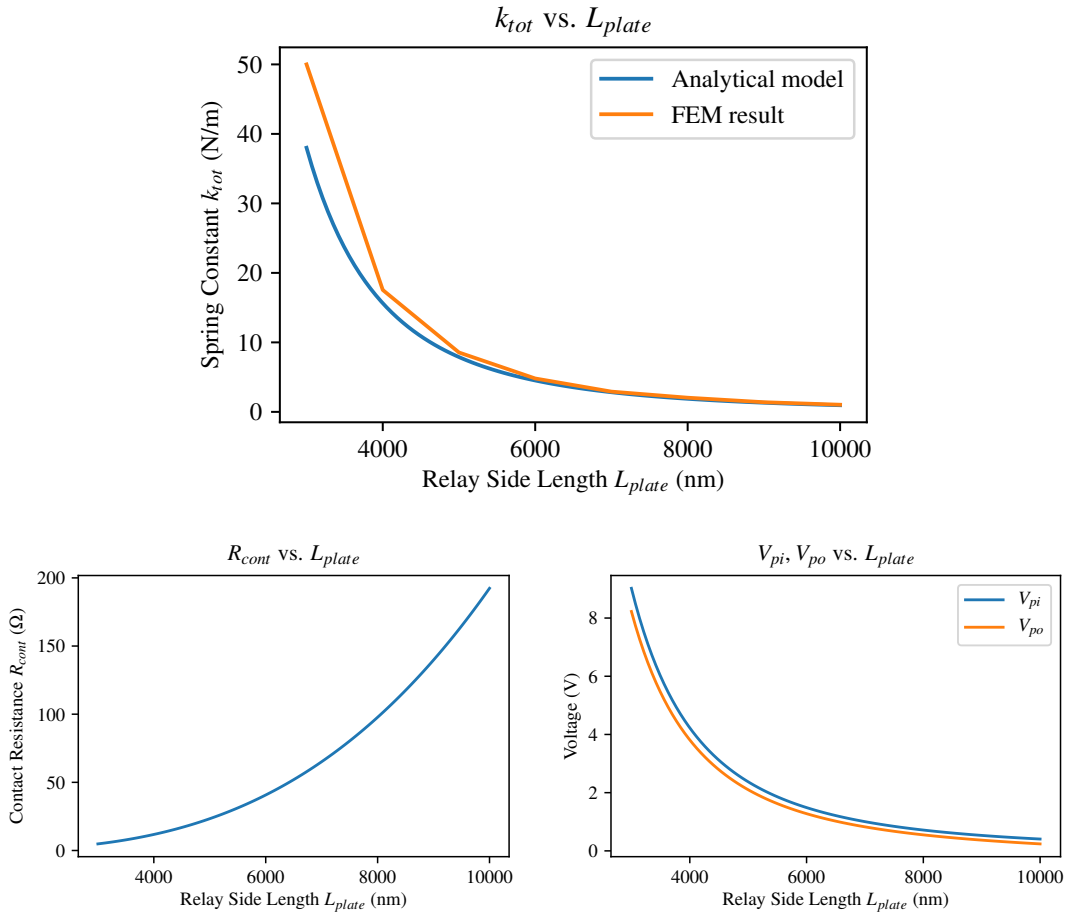

Figure 9: (Top) Spring constant of relay vs. relay side length. (Bottom Left) Contact resistance of relay vs. relay side length. (Bottom Right) Pull-in/pull-out voltage vs. relay side length. Cantilever beam lengths are constrained to be equal to the relay side length, and all other parameters are set to defaults.

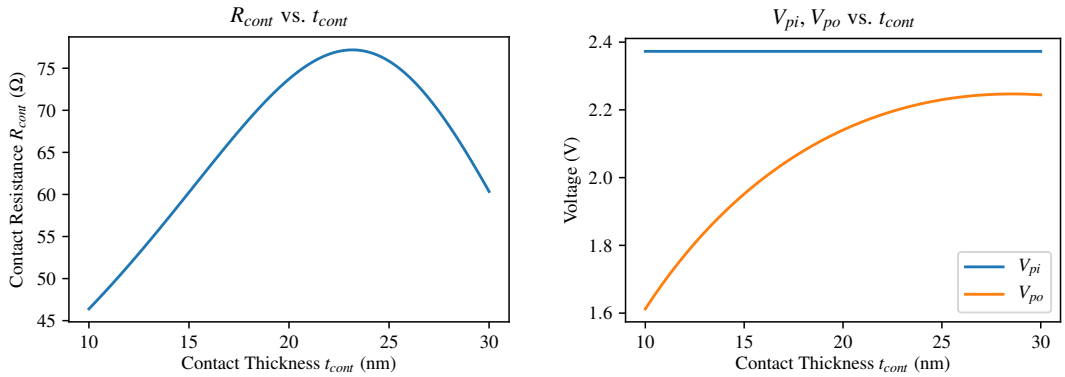

Figure 10: (Left) Contact resistance of relay vs. contact thickness. (Right) Pull-in/pull-out voltage vs. contact thickness. All other parameters are set to defaults.

affecting these parameters is through modification of both the actuation gap and the distance needed for contact to be made. The contact resistance is maximized at a critical contact thickness, while the V_{pi} remains constant. The V_{po} increases, which makes sense since thicker contacts mean the relay is further from the body in the ON state.

5.3.5 Poly-SiGe Thickness

The poly-SiGe thickness is one of the most important mechanical parameters of the relay. It affects the spring constant, which affects the pull-in/pull-out voltages, in turn affecting the contact resistance. This is shown in Figure 11. We first notice that the spring constant increases. This makes sense since thicker beams tend to have higher spring constants. As a result, we see that the pull-in and pull-out voltages increase since there is a stronger restoring force from the cantilever springs. The strong restoring force also results in a lower F_{net} which reduces the contact resistance as the cantilever beams get thicker.

5.3.6 Cantilever Width

The cantilever width is one of the most important mechanical parameters of the relay. It affects the spring constant, which affects the pull-in/pull-out voltages, in turn affecting the contact resistance. This is shown in Figure 12. We first notice that the spring constant increases. This makes sense since thicker beams tend to have higher spring constants. The agreement between the FEM result and the analytical model is very good. We see that the pull-in and pull-out voltages increase, since there is a stronger restoring force from the cantilever springs. The strong restoring force also results in a lower F_{net} which reduces the contact resistance as the cantilever beams are thickened.

6 Conclusion

The parametric multi-pole relay design presented here is CMOS compatible and operates at low voltages while maintaining a low contact resistance. It will be therefore be useful for programmable routers in PLDs. We analyze the effects of varying different system parameters with our approximate models as well as finite element models. All of our work is available under the MIT license on GitHub[1].

[1]https://github.com/akashlevy/NEM-Relay-CAD

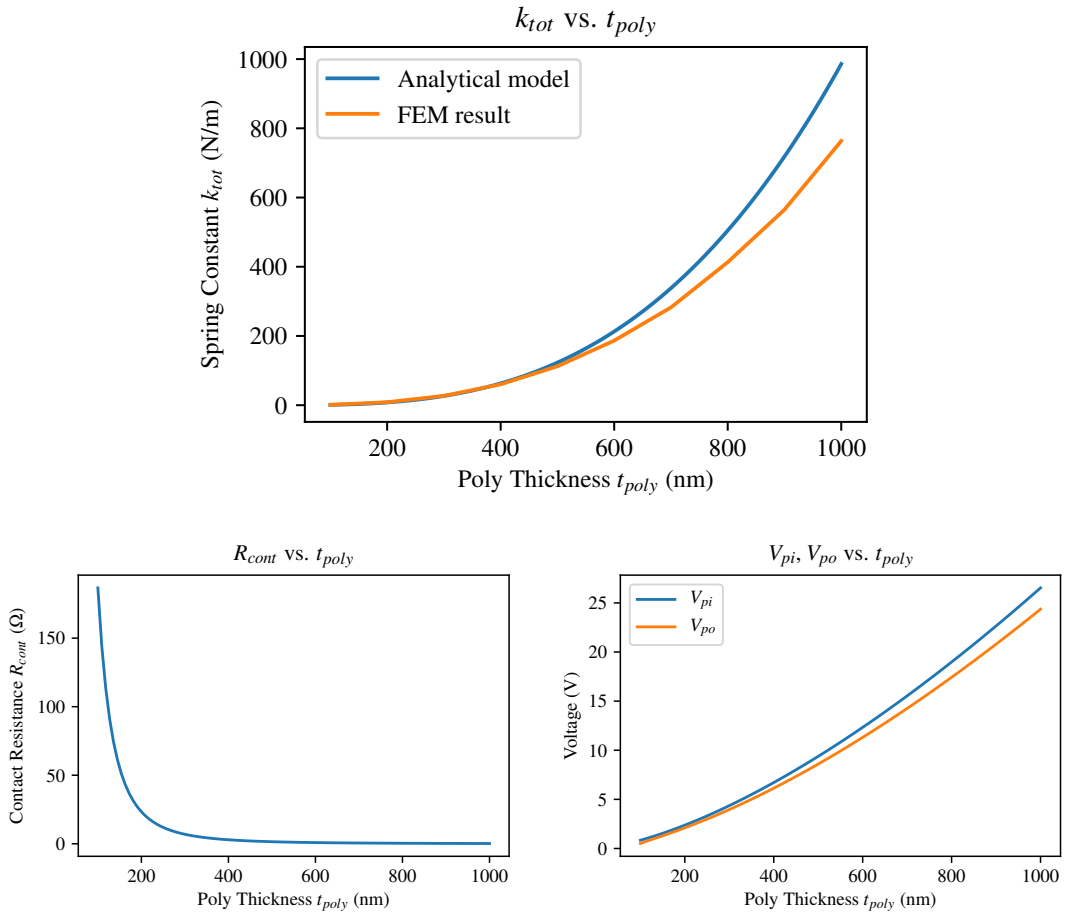

Figure 11: (Top) Spring constant of relay vs. poly-SiGe. (Bottom Left) Contact resistance of relay vs. poly-SiGe. (Bottom Right) Pull-in/pull-out voltage vs. poly-SiGe. All other parameters are set to defaults.

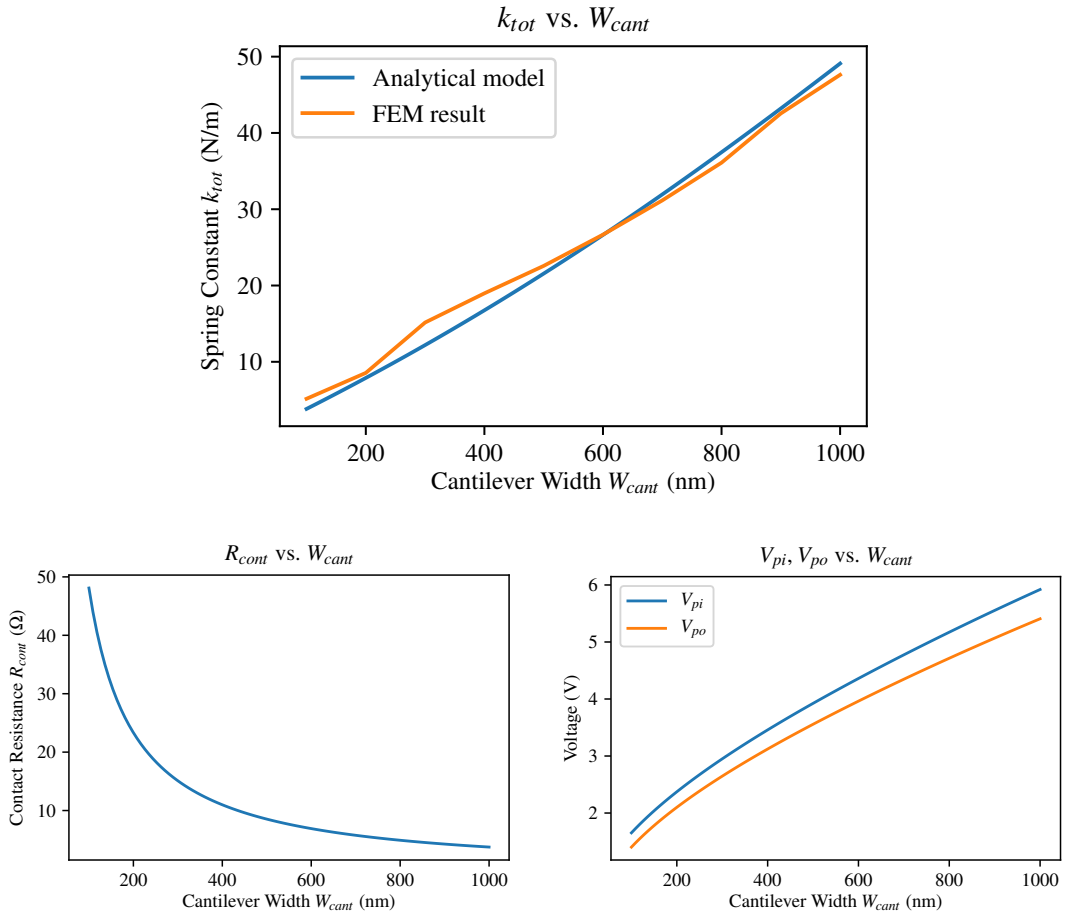

Figure 12: (Top) Spring constant of relay vs. cantilever width. (Bottom Left) Contact resistance of relay vs. cantilever width. (Bottom Right) Pull-in/pull-out voltage vs. cantilever width. All other parameters are set to defaults.

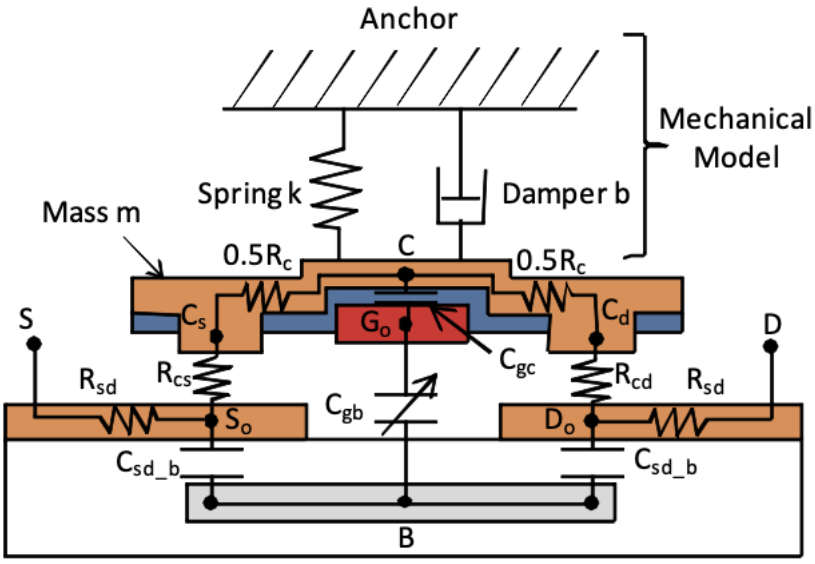

Figure 13: Adapted from [4]. A lumped SPICE model of a 4T NEM relay that incorporates the device's electro-mechanical behavior as well as parasitic resistances and capacitances.

6.1 Future Directions

Future work includes developing approximate Verilog-A SPICE models automatically from the layouts based on lumped models, such as that shown in Figure 13. Plugging these models into PLD designs and analyzing the effects could produce very interesting results for reducing reconfigurability overhead in these systems. Additionally, more work could be done with FEM tools to analyze pull-in/pull-out voltages and spring constants with more accuracy—better meshes could be used, capacitive shielding effects could be solved for accurately, and squeeze film damping could be accounted for. More work could also be done to analyze how relay parameters affect key figures of merit of programmable routing switches—in particular, power, switching delay, propagation delay, and area. Catastrophic pull-in voltages (where the relay collapses onto the body) need to be computed to determine whether the relay designs are truly feasible. Currently our OpenSCAD model does not allow modification of the beam length independently of the relay side length. This would be a good feature to add. Additionally, the routing of the contacts to vias is not available. This would be critical for making our designs layout-ready. In this study, we explore only one contact resistance model—however, others exist and may more accurately describe our system. These could be investigated. Other contact materials besides W could be investigated as well. Lastly, mechanical stress in the beam should be analyzed to determine the expected endurance of the relays.

References

[1] S. C. Bromley and B. J. Nelson. Performance of microcontacts tested with a novel mems device. In *Proceedings of the Forth-Seventh IEEE Holm Conference on Electrical Contacts (IEEE Cat. No. 01CH37192)*, pages 122–127. IEEE, 2001.

[2] C. Chen, W. S. Lee, R. Parsa, S. Chong, J. Provine, J. Watt, R. T. Howe, H.-S. P. Wong, and S. Mitra. Nano-electro-mechanical relays for FPGA routing: Experimental demonstration and a design technique. In *Design, Automation & Test in Europe Conference & Exhibition (DATE), 2012*, pages 1361–1366. IEEE, 2012.

[3] C. Chen, R. Parsa, N. Patil, S. Chong, K. Akarvardar, J. Provine, D. Lewis, J. Watt, R. T.

Howe, H.-S. P. Wong, et al. Efficient FPGAs using nanoelectromechanical relays. In *Proceedings of the 18th annual ACM/SIGDA international symposium on Field programmable gate arrays*, pages 273–282. ACM, 2010.

[4] F. Chen, H. Kam, D. Markovic, T.-J. K. Liu, V. Stojanovic, and E. Alon. Integrated circuit design with NEM relays. In *Proceedings of the 2008 IEEE/ACM International Conference on Computer-Aided Design*, pages 750–757. IEEE Press, 2008.

[5] K. L. Harrison, W. A. Clary, J. Provine, and R. T. Howe. Back-end-of-line compatible poly-SiGe lateral nanoelectromechanical relays with multi-level interconnect. *Microsystem Technologies*, 23(6):2125–2130, 2017.

[6] R. Holm. *Electric contacts: theory and application*. Springer Science & Business Media, 2013.

[7] H. Kam, V. Pott, R. Nathanael, J. Jeon, E. Alon, and T.-J. K. Liu. Design and reliability of a micro-relay technology for zero-standby-power digital logic applications. In *2009 IEEE International Electron Devices Meeting (IEDM)*, pages 1–4. IEEE, 2009.

[8] I. Kuon, R. Tessier, J. Rose, et al. FPGA architecture: Survey and challenges. *Foundations and Trends in Electronic Design Automation*, 2(2):135–253, 2008.

[9] T.-J. K. Liu, L. Hutin, I.-R. Chen, R. Nathanael, Y. Chen, M. Spencer, and E. Alon. Recent progress and challenges for relay logic switch technology. In *2012 Symposium on VLSI Technology (VLSIT)*, pages 43–44. IEEE, 2012.

[10] R. Nathanael, V. Pott, H. Kam, J. Jeon, and T.-J. K. Liu. 4-terminal relay technology for complementary logic. In *Electron Devices Meeting (IEDM), 2009 IEEE International*, pages 1–4. IEEE, 2009.

[11] M. Wijtvliet, L. Waeijen, and H. Corporaal. Coarse grained reconfigurable architectures in the past 25 years: Overview and classification. In *Embedded Computer Systems: Architectures, Modeling and Simulation (SAMOS), 2016 International Conference on*, pages 235–244. IEEE, 2016.

[12] S. S. Wong and A. El Gamal. The prospect of 3D-IC. In *Custom Integrated Circuits Conference, 2009. CICC'09. IEEE*, pages 445–448. IEEE, 2009.

[13] Z. Zhang, Y. Y. Liauw, C. Chen, and S. S. Wong. Monolithic 3-D FPGAs. *Proceedings of the IEEE*, 103(7):1197–1210, 2015.